



OPEN

Cannabis compounds exhibit anti-inflammatory activity in vitro in COVID-19-related inflammation in lung epithelial cells and pro-inflammatory activity in macrophages

Seeghalli M. Anil^{1,4}, Nurit Shalev^{1,4}, Ajampura C. Vinayaka^{1,4}, Stalin Nadarajan^{1,4}, Dvora Namdar¹, Eduard Belausov¹, Irit Shoval², Karthik Ananth Mani³, Guy Mechrez³ & Hinanit Koltai¹✉

Cannabis sativa is widely used for medical purposes and has anti-inflammatory activity. This study intended to examine the anti-inflammatory activity of cannabis on immune response markers associated with coronavirus disease 2019 (COVID-19) inflammation. An extract fraction from *C. sativa* Arbel strain (F_{CBD}) substantially reduced (dose dependently) interleukin (IL)-6 and -8 levels in an alveolar epithelial (A549) cell line. F_{CBD} contained cannabidiol (CBD), cannabigerol (CBG) and tetrahydrocannabinol (THCV), and multiple terpenes. Treatments with F_{CBD} and a F_{CBD} formulation using phytocannabinoid standards ($F_{\text{CBD:std}}$) reduced IL-6, IL-8, C-C Motif Chemokine Ligands (CCLs) 2 and 7, and angiotensin I converting enzyme 2 (ACE2) expression in the A549 cell line. Treatment with F_{CBD} induced macrophage (differentiated KG1 cell line) polarization and phagocytosis in vitro, and increased CD36 and type II receptor for the Fc region of IgG (FcγRII) expression. F_{CBD} treatment also substantially increased IL-6 and IL-8 expression in macrophages. $F_{\text{CBD:std}}$, while maintaining anti-inflammatory activity in alveolar epithelial cells, led to reduced phagocytosis and pro-inflammatory IL secretion in macrophages in comparison to F_{CBD} . The phytocannabinoid formulation may show superior activity versus the cannabis-derived fraction for reduction of lung inflammation, yet there is a need of caution proposing cannabis as treatment for COVID-19.

Coronavirus disease 2019 (COVID-19) is an acute resolved disease following infection by SARS-CoV-2 with a mortality of ~3.7%. The leading cause of COVID-19 mortality is respiratory failure due to acute respiratory distress syndrome¹. The disease progression of COVID-19 is often characterized by a two-phase immune response. A specific adaptive immune response is required during the first phase to eliminate the virus and to prevent disease progression to the more severe stage². Therefore, development of strategies to increase the immune response during this first stage are critical.

The second phase is usually associated with a virally-induced cytokine storm syndrome^{1,2}. The cytokine storm syndrome is characterized by elevated levels of several cytokines including interleukin (IL)-6 and IL-8, tumor necrosis factor alpha (TNFα) and C-C Motif Chemokine Ligand 2 (CCL2)³. Specific to the respiratory system, lung epithelial cells have been suggested to play a crucial role in the release of several pro-inflammatory cytokines including IL-6 and IL-8⁴.

¹Institute of Plant Science, Agriculture Research Organization, Volcani Center, 7528809 Rishon LeZion, Israel. ²The Mina & Everard Goodman Faculty of Life Sciences, Bar-Ilan University, 5290002 Ramat Gan, Israel. ³Institute for Postharvest and Food Science, Agriculture Research Organization, Volcani Center, 7528809 Rishon LeZion, Israel. ⁴These authors contributed equally: Seeghalli M. Anil, Nurit Shalev, Ajampura C. Vinayaka and Stalin Nadarajan. ✉email: hkoltai@agri.gov.il

Cannabis sativa is widely used for medical purposes. Cannabis strains produce more than 500 compounds, including phytocannabinoids, terpenes and flavonoids^{5–7}. Cannabinoids have been suggested to be immune modulators and to change the balance between pro- and anti-inflammatory cytokines^{8,9}. Cannabinoids can also influence macrophage activity. For example, Δ^9 -tetrahydrocannabinol (THCV) inhibits nitrite production and IL-1 β protein levels in lipopolysaccharide activated macrophages¹⁰. Further, Δ^9 -tetrahydrocannabinol (THC) can inhibit macrophage phagocytosis by 90%¹¹. Cannabidiol (CBD) is also suggested to have anti-inflammatory effects in various conditions¹². For example, CBD increases intracellular calcium levels in rheumatoid arthritis synovial fibroblasts and reduces the production of IL-6 and IL-8¹². Because CBD shows anti-inflammatory activity, and is approved by the Food and Drug Administration (FDA) for the treatment of children with intractable epilepsy for seizure reduction, it has been suggested that CBD might alleviate COVID-19 related inflammation¹³. However, little is known regarding the effect of different cannabis compounds or their combinations on alveolar epithelial and immune cell inflammation.

Here, we identified cannabis compounds that exhibit anti-inflammatory activity in lung epithelial cells, yet substantially induce polarization, phagocytosis and IL expression in macrophages in vitro.

Results

Cannabis crude extract and fractions reduce the level of IL-8 and IL-6 in lung epithelial cell model. Inflorescence extracts of the high CBD *C. sativa* strain Arbel were used to examine cannabis activity in reducing TNF α induced inflammation in the lung epithelial cancer cell line A549.

The crude extract led to a substantial reduction of IL-6 and IL-8 secretion levels at 5 $\mu\text{g}/\text{mL}$ (Fig. 1a,b). Subsequently, high CBD (F_{CBD}) and high THC (F_{THC}) fractions were examined for their anti-inflammatory activity (Fig. 1a, Supplementary Fig. S1). F_{THC} exhibited only low anti-inflammatory activity; however, F_{CBD} showed considerable activity in the reduction of IL-6 and IL-8 secretion levels from lung epithelial cells, with an IC_{50} of 3.45 and 3.49 $\mu\text{g}/\text{mL}$ respectively (Fig. 1c,d). F_{CBD} reduced IL-8 levels more than dexamethasone at 4 $\mu\text{g}/\text{mL}$, and reduced IL-6 and IL-8 to levels similar to that of the crude extract (Fig. 1a,b). The crude extract and F_{THC} led to substantial cell death (61 and 42% viability, respectively), whereas F_{CBD} at 5 $\mu\text{g}/\text{mL}$ was comparatively less cytotoxic (76.7% viability; Supplementary Fig. S2).

CBD (the main phytomolecule in F_{CBD}) treatment alone exhibited an inverted bell shaped activity curve, i.e., 3.0 $\mu\text{g}/\text{mL}$ reduced both IL-6 and IL-8 levels, similar to F_{CBD} at 4.1 $\mu\text{g}/\text{mL}$ (Fig. 2a,b). Higher or lower concentrations of CBD showed lower and/or nonsignificant reduction of IL-6 and IL-8 levels (Fig. 2a,b).

The combination of phytocannabinoid standards at the ratios found in fraction F_{CBD} ($F_{\text{CBD:std}}$) showed similar activity to F_{CBD} in the lung epithelial cell model. Based on high-performance liquid chromatography (HPLC) and gas chromatography–mass spectrometry analysis, F_{CBD} contains approximately 66% phytocannabinoids by total content. The phytocannabinoid assemblage included CBD (93.5%), CBG (6.1%) and a minute amount of THCV (0.4%) (Table 1; Supplementary Fig. S1). Additionally, multiple terpenes were detected in F_{CBD} (Table 1; Supplementary Fig. S3). A combination of phytocannabinoid standards at the ratios found in fraction F_{CBD} ($F_{\text{CBD:std}}$) resulted in activity similar to that of the cannabis-derived fraction (IC_{50} of 4.1 $\mu\text{g}/\text{mL}$ for IL-6 and IL-8; Fig. 1e,f).

CB2 inverse agonist attenuated F_{CBD} and $F_{\text{CBD:std}}$ activity in lung epithelial cell model. Treatment with CB1 or CB2 inverse agonists (IA), TRPA1 blocker, TRPV1 or TRPV2 receptor antagonists did not affect F_{CBD} or $F_{\text{CBD:std}}$ activity on IL-6 secretion (Fig. 3a). Using CB2 IA and TRPV1 and TRPV2 antagonists to a lesser extent, with $F_{\text{CBD:std}}$ treatments increased IL-8 secretion in A549 cells in comparison to $F_{\text{CBD:std}}$ alone (Fig. 3b). CB1 and CB2 IA, TRPA1 blocker or TRPV1 or TRPV2 receptor antagonists did not affect F_{CBD} activity on IL-8 secretion (Fig. 3b). Treatment with CB2 IA, TRPA1 blocker or TRPV1 or TRPV2 receptor antagonists did not affect IL-6 or IL-8 levels, except for CB1 IA that led to reduction in IL-8 and IL-6 levels (Fig. 3; Supplementary Fig. S4).

F_{CBD} treatment lead to reduction in *CCL2*, *CCL7*, *ACE2* and *IL-7* gene expression in lung epithelial cell model. Quantitative PCR analysis demonstrated that F_{CBD} or $F_{\text{CBD:std}}$ treatments reduced the mRNA steady state level of the pro-inflammatory cytokines *CCL2* and *CCL7* in TNF α treated A549 cells (Fig. 4a,b). However, the reduced expression of the two genes was less than those treated with dexamethasone (Fig. 4a,b). $F_{\text{CBD:std}}$ treatment led to only a 1.3-fold reduction in the expression level of *IL-7*, whereas F_{CBD} and dexamethasone reduced *IL-7* expression substantially (2.6- and 2.7-fold, respectively; Fig. 4c). Moreover, F_{CBD} , $F_{\text{CBD:std}}$ and dexamethasone treatments reduced the expression level of *angiotensin 1 converting enzyme 2 (ACE2)*, F_{CBD} to a greater extent than dexamethasone or $F_{\text{CBD:std}}$ (Fig. 4d). Expression levels of these genes were examined also at 4 h post- F_{CBD} treatment. F_{CBD} reduction of *CCL2* and *CCL7* gene expression was not apparent at 4 h, although at 4 h F_{CBD} treatment substantially reduced *ACE-2* and *IL-7* expression levels (Supplementary Fig. S5).

F_{CBD} and $F_{\text{CBD:std}}$ treatments induce *IL-6*, *IL-8* and *CCL2* expression in a differentiated KG1 cell line. F_{CBD} treatment increased *IL-6*, *IL-8* and *CCL2* expression in phorbol-12-myristate-13-acetate (PMA)-treated (differentiated KG1 cells) macrophages by ~2-, ~433- and ~49-fold, respectively (Fig. 5a–c). $F_{\text{CBD:std}}$ increased *CCL2* expression by ~20-fold (Fig. 5c) and *IL-8* expression level by ~26-fold (Fig. 5b); however $F_{\text{CBD:std}}$ did not lead to increased *IL-6* expression in macrophages (Fig. 5a). At the protein level in KG1 treated with TNF α , F_{CBD} but not $F_{\text{CBD:std}}$ increased IL-8 secretion in macrophages (Fig. 5d). F_{CBD} activity was dose dependent (Fig. 5e). Dexamethasone (at 8 and 4 $\mu\text{g}/\text{mL}$) did not decrease expression of *IL-6*, *IL-8*, *CCL2*, or IL-8 secretion in macrophages (Fig. 5a–e, respectively).

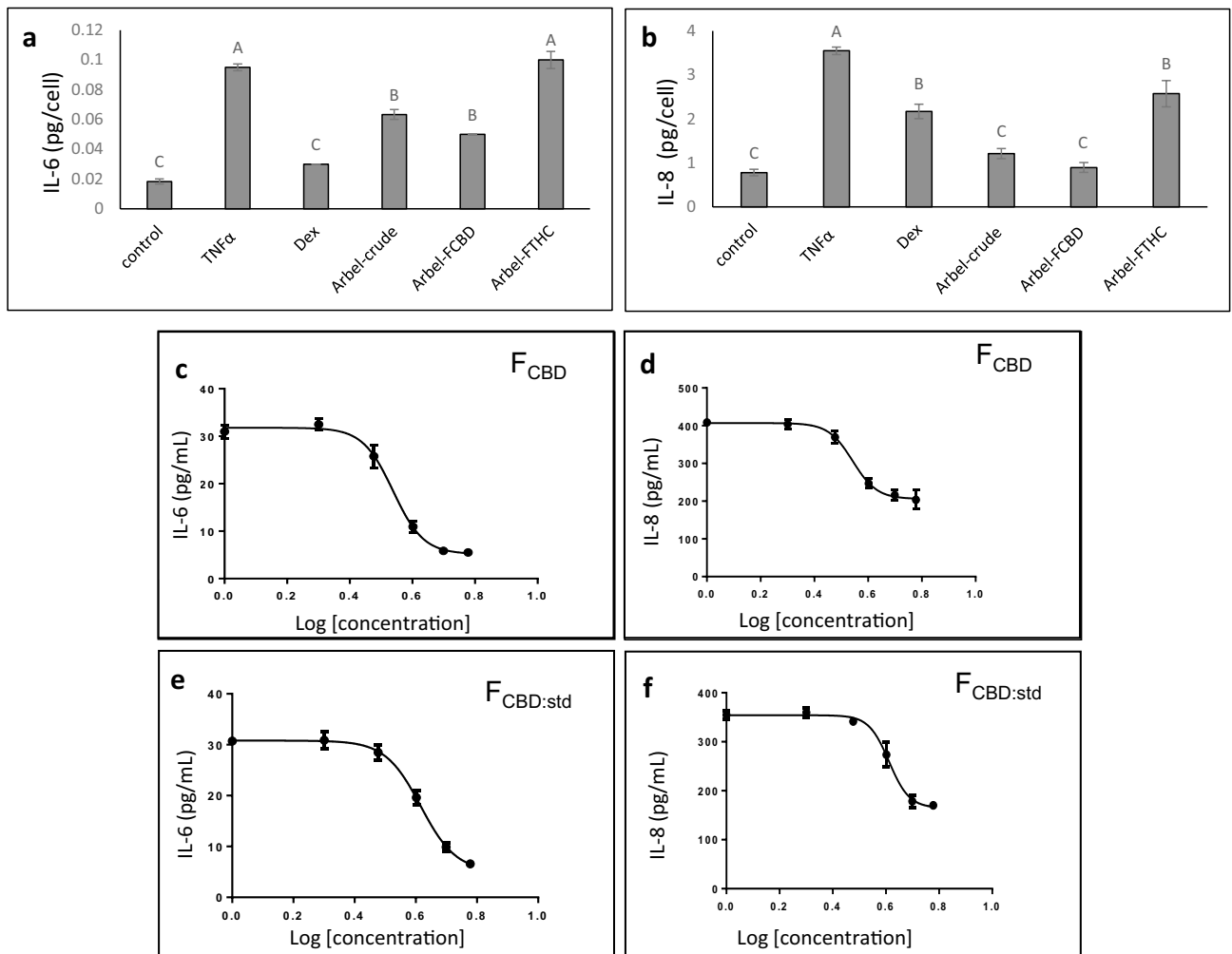


Figure 1. The levels of (a) IL-6 and (b) IL-8 in A549 cells treated with *C. sativa* Arbel crude and F_{CBD} and F_{THC} extract fractions. Cells were treated with 300 ng/mL TNFα and *C. sativa* extract and fractions at a concentration of 5 μg/mL for 4 h. Dexamethasone (Dex; 4 μg/mL) served as a positive control. Control (0.5% v/v methanol) treatment served as the solvent (vehicle) control; TNFα indicates TNFα+ solvent control treatment. Error bars indicate ± standard error (sem) (n = 3). Bars labeled with different letters are significantly different from all combinations of pairs by Tukey–Kramer honest significant difference test (HSD; $P \leq 0.05$). Dose–effect curves of *C. sativa* F_{CBD} on (c) IL-6 and (d) IL-8 levels in the A549 cell line. Dose–effect curves of F_{CBD:std} (93.5% CBD+6.1% CBG+0.4% THCv) on (e) IL-6 and (f) IL-8 levels in the A549 cell line. GraphPad Prism version 6.1 was used to produce the dose–response curve and IC₅₀ doses. Error bars indicate ± sem (n = 3).

F_{CBD} and F_{CBD:std} attenuate macrophages polarization. To examine the effect of the treatments on macrophage phagocytosis we incubated PMA-treated macrophages with fluorescent-labeled silica 50–100 nm particles (FNP). In the control, most of the cells were non-polarized and featured a round structure (Table 2; Fig. 6), whereas the macrophage population treated for 16 h with F_{CBD} (7 μg/mL) consisted of ~48% polarized cells (Table 2). Multiple silica particles and membrane pseudopods were detected in the polarized cells (Fig. 6). Likewise, treatment of the macrophage population with F_{CBD:std} resulted in ~49% polarized cells (Table 2). Lower concentrations of F_{CBD} (3.5 μg/mL) led to a somewhat reduced percentage of polarized cells (~45%) and macrophage treatment with CBD at the equivalent concentration (4.35 μg/mL) found in F_{CBD} 7 μg/mL resulted in only ~18% polarized cells.

F_{CBD} and F_{CBD:std} attenuate expression of phagocytosis-associated receptors. F_{CBD} treatment, but not F_{CBD:std}, increased expression of *FcγRII* and *CD36* in comparison to the vehicle control (Fig. 7a,b). Treatment with ruxolitinib which inhibits monocyte activation (described by Ahmed et al.¹⁴) reduced *FcγRII* expression (Fig. 7a), and palmitic acid (PA) reduced expression of *CD36* (Fig. 7b), in agreement with¹⁵. Expression of *SCARB1* was reduced by F_{CBD} and ruxolitinib, but not by F_{CBD:std} (Fig. 7c).

F_{CBD} increases silica particle internalization in macrophages. Imaging flow cytometry analysis showed that F_{CBD} increased the percentage of macrophage cells that internalized FNP (Table 3; Supplementary

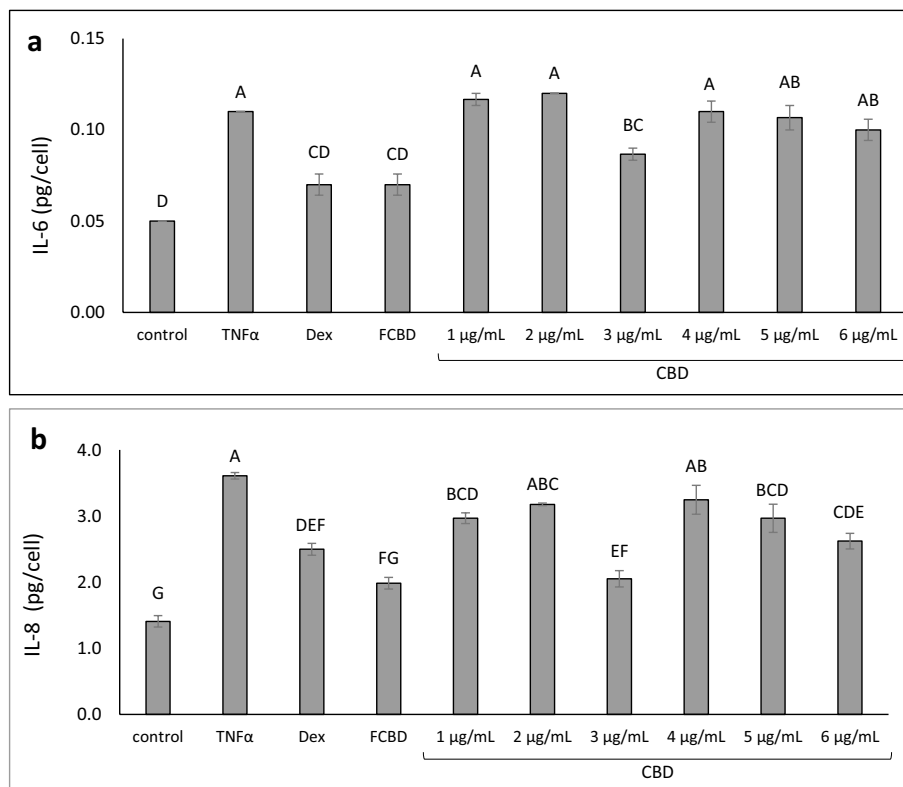


Figure 2. The level of (a) IL-6 and (b) IL-8 in A549 cells treated with F_{CBD} and CBD. Cells were treated with 300 ng/mL TNF α , 4.1 $\mu\text{g/mL}$ F_{CBD} (FCBD) and CBD at different concentrations for 4 h. Dexamethasone (Dex; 4 $\mu\text{g/mL}$) served as a positive control. Control (0.6% v/v methanol) treatment served as the solvent (vehicle) control; TNF α is TNF α + solvent control treatment. Error bars indicate \pm sem (n = 3). Bars labeled with different letters are significantly different from all combinations of pairs according to the Tukey–Kramer HSD test ($P \leq 0.05$).

Phytocannabinoids	% of phytocannabinoids	% of total
CBD	93.5	61.7
CBG	6.1	4.0
THCV	0.4	0.3
Terpenes	% of terpenes	% of total
Butylated hydroxytoluene	2.6	0.3
1,6-Dioxacyclododecane-7,12-dione	1	0.1
Guaiol	10.4	1.2
γ -Eudesmol	2.3	0.3
α -Eudesmol	5.6	0.6
Guaienol	1.3	0.2
γ -Curcumene	75.6	8.7
Other	1.2	0.1

Table 1. Terpene and phytocannabinoids composition in F_{CBD} as a percentage of total phytocannabinoids/terpenes and as a percentage of total compounds in extract.

Fig. S6). The increase in percentage of positive cells by F_{CBD} was higher in comparison to the vehicle control also for the fluorescent-labeled silica 30–70 nm particles (ENP) and for the IgG coated, fluorescent-labeled silica 30–70 nm particles (ENPG). $F_{\text{CBD:std}}$ and CBD treatments were less effective in increasing internalization (for FNP) or presence (ENP and ENPG) of the particles in cells in comparison to the F_{CBD} treatment (Table 3; Supplementary Fig. S6).

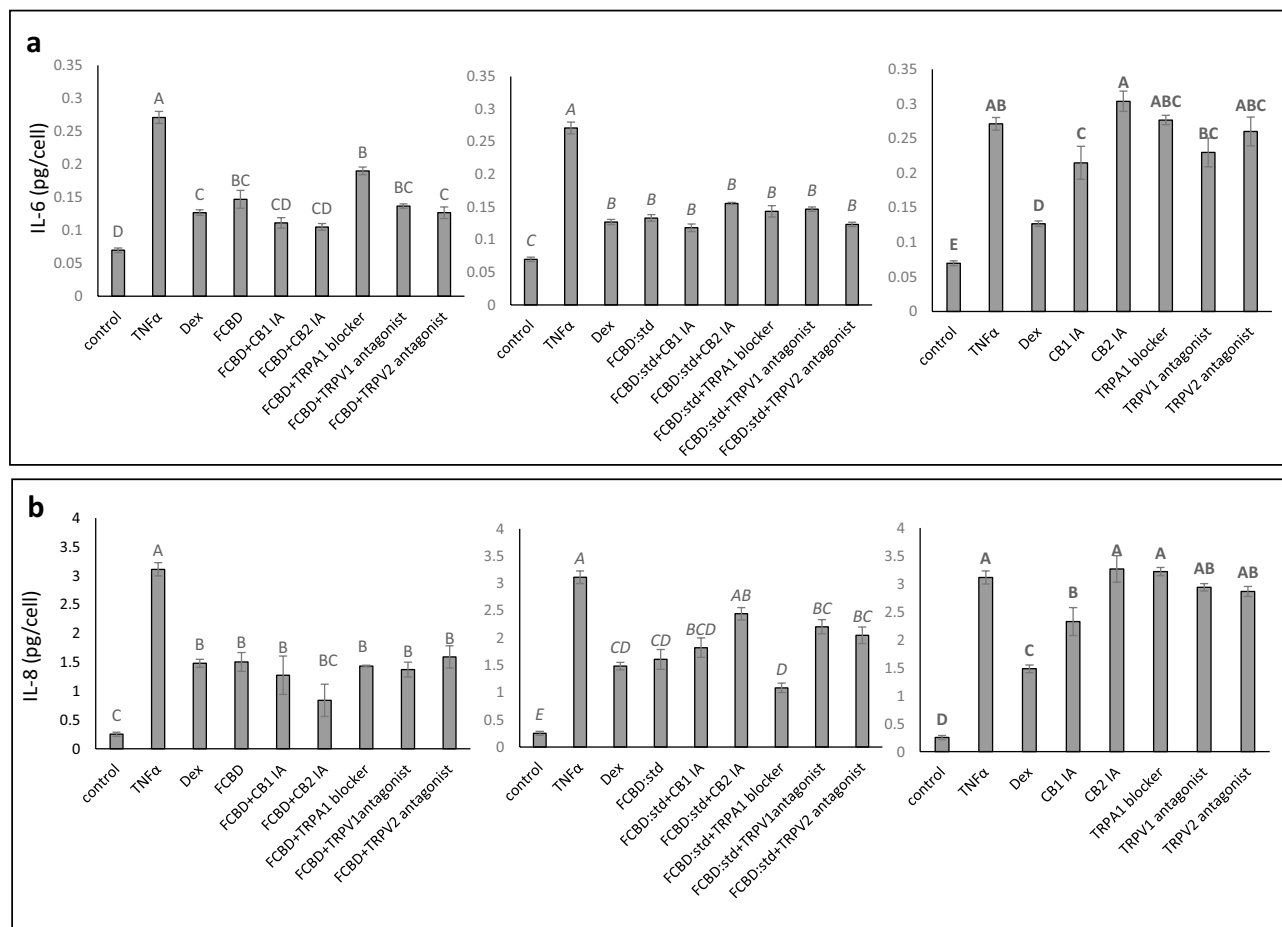


Figure 3. Levels of (a) IL-6 and (b) IL-8 in A549 cells treated with F_{CBD} or $F_{\text{CBD:std}}$ with or without CB1 or CB2 inverse agonists (IA), TRPA1 blocker, or TRPV1 or TRPV2 antagonists. Cells were treated with 300 ng/mL TNF α and F_{CBD} (FCBD) and $F_{\text{CBD:std}}$ (FCBD:std) at a concentration of 3.4 and 4.1 $\mu\text{g}/\text{mL}$, respectively, in the presence or absence of IA of CB1 (5 μM) or CB2 (5 and 7.5 μM for IL-6 and IL-8, respectively), a TRPA1 blocker (10 μM), or TRPV1 or TRPV2 antagonists (10 μM) for 4 h. Dexamethasone (Dex) served as a positive control at 4 $\mu\text{g}/\text{mL}$. Control (0.4% v/v methanol + 2% v/v dimethyl sulfoxide [DMSO]) treatment served as the solvent (vehicle) control; TNF α is TNF α +solvent control treatment. Error bars indicate \pm sem ($n=3$). Bars labeled with different letters are significantly different from all combinations of pairs according to the Tukey–Kramer HSD test ($P\leq 0.05$).

Discussion

We have identified a CBD rich fraction (F_{CBD}) from the inflorescence extract of a high CBD cannabis strain with immune-modulation activity in alveolar epithelial and macrophage cell models. F_{CBD} reduced IL-8 and IL-6 secretion in alveolar epithelial cells. IL-8 is one of the cytokines that characterizes the cytokine storm in severe COVID-19 patients; IL-6 is a prominent cytokine also involved in the cytokine storm and is secreted during the disease from alveolar epithelial cells³. In addition to CBD, F_{CBD} contained CBG and minute amount of THCv. The IC_{50} of a combinations of active phytocannabinoid standards ($F_{\text{CBD:std}}$) at the relative concentrations found in F_{CBD} were similar to that of the original fraction in the alveolar epithelial cell model.

Treatment with CBD by itself led to a reduction in IL-6 and IL-8 levels in an inverse bell-shaped dose–response in alveolar epithelial cells; i.e., only 3 $\mu\text{g}/\text{mL}$ was active whereas other CBD concentrations exhibited lower or no cell activity. These results are in line with an earlier publication suggesting that CBD has a bell-shaped dose–response for anti-inflammatory activity by Gallily et al.¹⁶. Notably, F_{CBD} (i.e., combination of CBD with CBG and THCv) led to a dose-dependent response rather than a bell-shaped dose–response. These results are in accordance with¹⁶, suggesting that the addition of other phytomolecules to CBD (crude cannabis extract in the case of¹⁶) prevented its bell-shaped dose–response. The CBD bell-shaped dose–response is associated with a narrow therapeutic window, which is difficult to use effectively in clinical therapy. Therefore, the fact that F_{CBD} has a dose-dependent response makes it better suited than CBD for patient care.

CBD is a negative allosteric modulator of CB1 signaling¹⁷. TRPA1 is a receptor in alveolar epithelial cells involved in the pathogenesis of several airway diseases including chronic obstructive pulmonary disease and asthma¹⁸. Both TRPV1 and TRPV2 interact with phytocannabinoids, including CBD, CBG and THCv¹⁹. Also, TRPV1, TRPV2 and TRPA1 were found to be associated with pulmonary inflammation²⁰. Nevertheless, co-treatment with CB1 IA, TRPA1 blocker or TRPV1 or TRPV2 antagonist had no substantial effect on F_{CBD} and

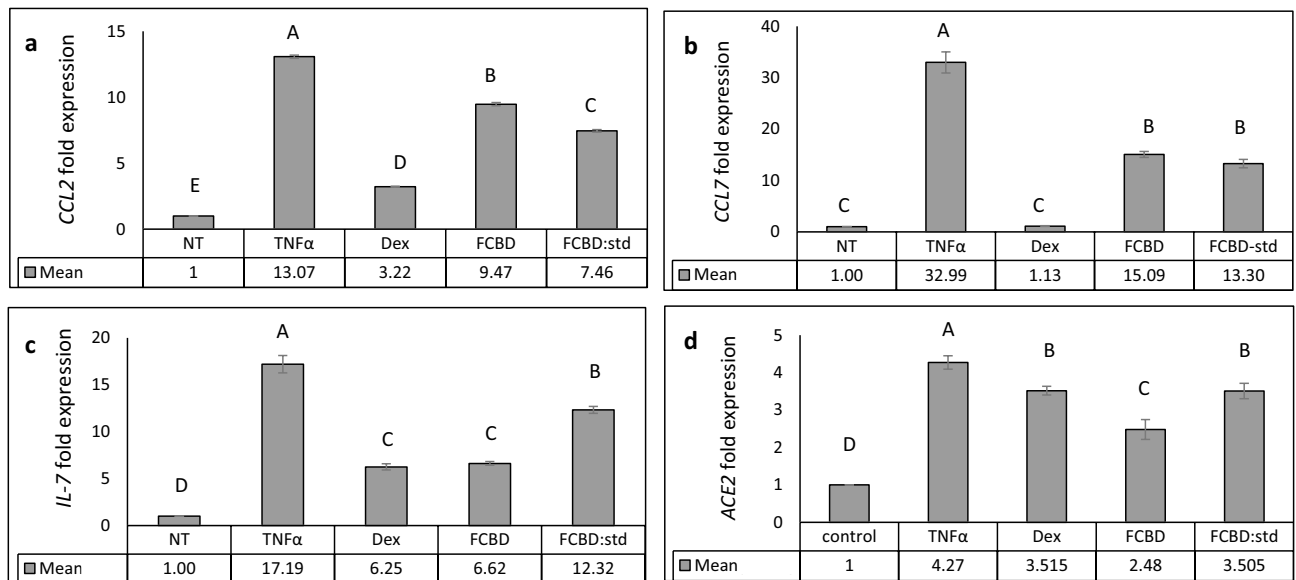


Figure 4. qPCR-based determination of the mRNA steady state level in A549 cell line of (a) *CCL2*, (b) *CCL7*, (c) *IL-7* or (d) *ACE2* genes, after treatment with TNF α (300 μ g/mL), F_{CBD} (FCBD; 7 μ g/mL) or F_{CBD:std} (FCBD:std; 7 μ g/mL), or Dexamethasone (Dex; 4 μ g/mL)—for 6 h relative to the control. Control (0.7% v/v methanol) treatment served as the solvent (vehicle) control; TNF α indicates TNF α +solvent control treatment. Error bars indicate \pm sem (n = 3). Bars labeled with different letters are significantly different from all combinations of pairs according to the Tukey–Kramer HSD test (HSD; $P < 0.05$).

F_{CBD:std} activity. Only co-treatment with CB2 IA affected F_{CBD:std} activity on IL-8 secretion. The involvement of receptors in F_{CBD} and F_{CBD:std} activity remains to be demonstrated.

In addition to reducing IL-6 and IL-8 levels, F_{CBD} and F_{CBD:std} reduced the expression levels of *CCL2* and *CCL7* in alveolar epithelial cells by 6 h treatment. The systemic cytokine profiles detected in severe COVID-19 patients includes increased production of inflammatory chemokines such as *CCL2*²¹. Moreover, *CCL2* and *CCL7* were shown to be abundant in bronchoalveolar fluid from severe COVID-19 patients and were associated with recruitment of monocytes into the lungs²¹. Our results suggest that treatment with F_{CBD} or F_{CBD:std} may lead to reduced secretion of inflammatory cytokines associated with the disease, and possibly to a reduction of macrophage recruitment during the cytokine storm. However, dexamethasone was more effective than F_{CBD} in reducing both *CCL2* and *CCL7* expression.

IL-7 was shown to raise lymphocyte counts in septic patients with low absolute lymphocyte counts²² and to restore protective immunity in patients that suffer from CD4+ T cell deficiency (e.g., as in the case of HIV infection²³). It was suggested that treatment against SARS-CoV-2 infections should also attempt to increase IL-7 levels²². The fact that F_{CBD:std} reduced *IL-7* expression only to a minor extent in comparison to dexamethasone or F_{CBD} suggests that using purified phytocannabinoids may have an advantage over cannabis-derived fractions for COVID-19-like inflammation.

The ACE2 receptor is a part of the dual renin-angiotensin system (RAS)²⁴. ACE2 was shown to be involved with SARS-CoV-2 human infection; the ectodomain of the S protein of SARS-CoV-1 binds to the peptidase domain of ACE2 with relatively high affinity²⁵. In cells of patients with severe symptoms of COVID-19, ACE2 was substantially upregulated 199-fold; this upregulation was suggested to be one of the factors leading to disruption of the RAS, as ACE2 is a part of the counteracting hypotensive axis of RAS. The increase in ACE2 and other key RAS components is predicted to elevate bradykinin levels in multiple tissues, leading to increases in vascular permeability and hypotension; the latter is highly associated with severe COVID-19 patients²⁶. Indeed, a negative correlation was identified between *ACE2* gene expression and COVID-19 mortality²⁷. F_{CBD} reduced the expression level of *ACE2* at 4 and 6 h post treatment. F_{CBD:std} and dexamethasone also reduced *ACE2* expression but to a lesser extent. However, the ability of F_{CBD} to reduce *ACE2* expression should be examined at both the protein and functional levels (e.g., binding of the viral protein) to fully determine the effect F_{CBD} may have on ACE2-related treatment of COVID-19 patients. In any case, such reduction of *ACE2* expression should be considered with care as the advantages and disadvantages of this reduction are disputed²⁴.

In the first phase of the disease, a specific adaptive immune response is needed to eliminate the virus and to prevent disease progression to more severe stages². Indeed, the dysfunction of alveolar macrophages are among the abnormal characteristics in some severe COVID-19 patients²⁸, and an abundance of increased inflammatory monocyte-derived macrophages replaces tissue-resident alveolar macrophages in patients with severe disease²¹. Additionally, during SARS-CoV-1 infections that provoke a disease course similar to those seen during infection with SARS-CoV-2²¹, a marked reduction in macrophages phagocytosis activity was detected²⁹. Also, phagocytosis was important in the antibody-mediated elimination of SARS-CoV-1 in a mouse model³⁰.

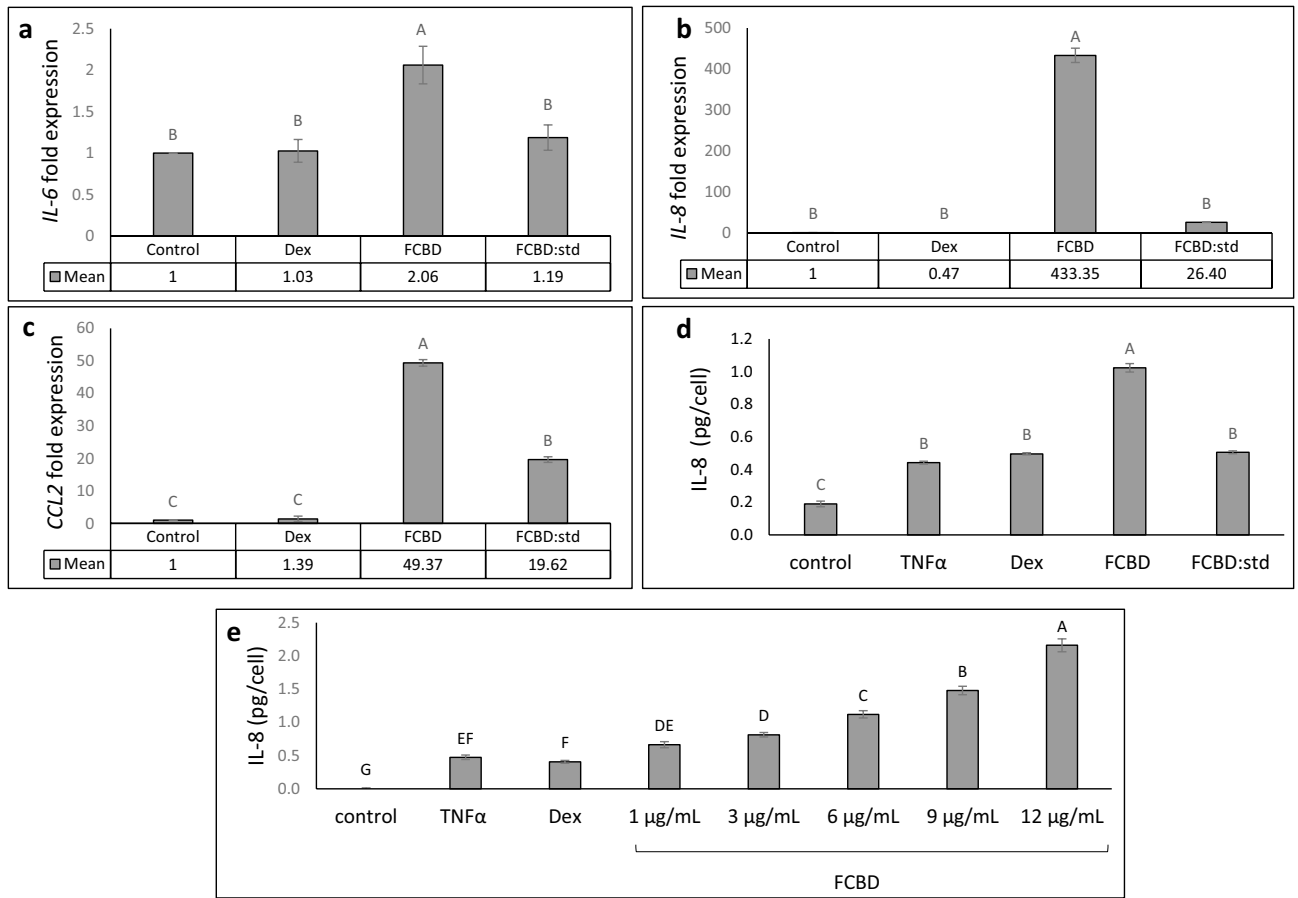


Figure 5. qPCR-based determination of the mRNA steady state level in the differentiated KG1 cell line of (a) *IL-6*, (b) *IL-8* or (c) *CCL2* after treatment with TNF α (300 μ g/mL), F_{CBD} (FCBD) at 7 μ g/mL, F_{CBD:std} (FCBD:std) at 7 μ g/mL and dexamethasone (Dex) at 8 μ g/mL for 6 h relative to control. Control (0.7% v/v methanol) treatment served as the solvent (vehicle) control. (d) *IL-8* levels in KG1 cells treated with F_{CBD} and F_{CBD:std}. Cells were treated with 300 ng/mL TNF α (and not by PMA), F_{CBD} (FCBD) or F_{CBD:std} (FCBD:std) at 10 μ g/mL for 6 h. Dexamethasone (Dex; 4 μ g/mL) served as a positive control. Control (1% v/v methanol) treatment served as the solvent (vehicle) control; TNF α is TNF α + solvent control treatment. (e) *IL-8* levels in KG1 cells treated with F_{CBD}. Cells were treated with 300 ng/mL TNF α (and not by PMA) and F_{CBD} at different concentrations for 6 h. Dexamethasone (Dex; 4 μ g/mL) served as a positive control. Control (1.2% v/v methanol) treatment served as the solvent (vehicle) control; TNF α indicates TNF α + solvent control treatment. Error bars indicate \pm sem (n = 3). Bars with different letters are significantly different from all combinations of pairs according to the Tukey–Kramer HSD test ($P \leq 0.05$).

Treatment	% of polarized cells	Total number of cells counted in all replicates (n = 5)
Control	1.2 \pm 0.83 ^b	204
F _{CBD} (7 μ g/mL)	48.3 \pm 6.9 ^a	144
F _{CBD:std} (7 μ g/mL)	48.8 \pm 11.3 ^a	74
CBD (4.3 μ g/mL)	17.9 \pm 4.1 ^{ab}	94
F _{CBD} (3.5 μ g/mL)	44.9 \pm 12.4 ^a	70

Table 2. Percentage of polarized cells out of the total differentiated KG1 cell population. Control (0.7% v/v methanol) treatment served as the solvent (vehicle) control. Means (n = 5 populations) labeled with different letters are significantly different from all combinations of pairs according to the Tukey–Kramer HSD test ($P \leq 0.05$).

Notably, F_{CBD} and F_{CBD:std}, and CBD to a lesser extent, led to a marked increase in macrophage polarization and to cell actin remodeling that corresponds to the growth of filopodia-like membrane structures³¹. F_{CBD} reduced expression of *SCARB1*; *SCARB1* encodes SR-B1 that is a scavenger receptor (class B) and is also responsible for phagocytosis of silica particles in macrophages³². However, F_{CBD} treatment also led to an increase in *FcyRII* and *CD36* gene expression. Phagocytosis is initiated by the ligation of Fcy receptors to IgG-opsonins on the target

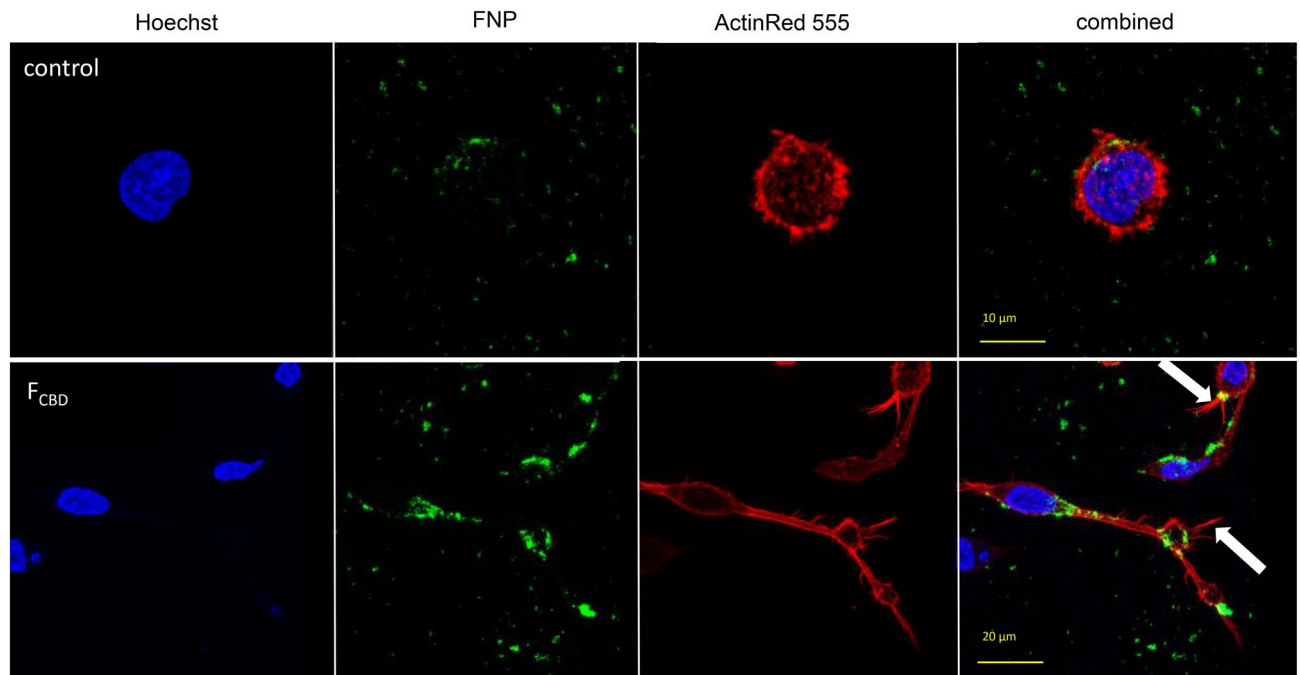


Figure 6. Representative examples of confocal images of macrophages following treatment with the control and F_{CBD} (7 $\mu\text{g}/\text{mL}$). Control (0.7% v/v methanol) treatment served as the solvent (vehicle) control. Cells were stained for F-actin (EasyProbes™ ActinRed 555 Stain, red stain), and nuclei (Hoechst, blue stain); $n = 5$, in each biological replicate multiple cells were examined (see Table 2). Membrane filopodia-like structures are marked with white arrows. FNP, fluorescent-labeled silica 50–100 nm particles.

cell³³, whereas CD36 expression in macrophages was shown to be involved with lung fibrosis in mice³⁴. Alveolar macrophages play an important role in Fc receptor-mediated responses during acute virus infections and in phagocytosis-mediated clearance of respiratory virus infections^{35,36}. CD36 is an important scavenger receptor for phagocytosis of *Streptococcus pneumoniae*, a primary bacterial agent associated with pneumonia, which is down regulated by influenza³⁷. Indeed, F_{CBD} led to a marked increase in the internalization of silica particles by macrophages, and in so doing, increased levels of phagocytosis.

Possibly, the increase in macrophage polarization and phagocytosis, and the upregulation of *FcγRII* and *CD36* expression in these cells following F_{CBD} treatment may facilitate phagocytosis-mediated clearance of respiratory viruses, and benefit the first phase of the immune response to SARS-CoV-2. However, it should be noted that macrophages themselves can be infected by the virus, as SARS-CoV-1 infects macrophages as a result of IgG-mediated phagocytosis that requires *FcγRII* receptor signaling pathways³⁸. Advantages and disadvantages of increasing macrophage phagocytosis activity should be carefully considered^{3,21}.

Notably, although $F_{\text{CBD:std}}$ treatment increased macrophage polarization, it did not increase the phagocytosis-associated gene expressions, nor phagocytosis. Hence, additional active compounds in the cannabis-derived F_{CBD} and not in the phytocannabinoid standard mix that composed $F_{\text{CBD:std}}$ are responsible for this increased gene expression and phagocytosis activity. Indeed, F_{CBD} contained multiple terpenes, some including γ -Curcumene and Guaiol at considerable percentages. The presence of terpenes in F_{CBD} may account for the differences in activity between F_{CBD} and $F_{\text{CBD:std}}$.

During the second phase of COVID-19, pneumonia patients exhibit features of macrophage activation syndrome (MAS) in which macrophages play a major pro-inflammatory role by releasing pro-inflammatory cytokines such as IL-6, IL-8 and CCL2³. Moreover, subsets of macrophages in patients with COVID-19 were found to express genes associated with IL-6, whereas expression of IL-6 was again associated with severe depletion of lymphocytes from the spleen and lymph nodes²¹. Notably, F_{CBD} led to a marked increase of *IL-8* expression and IL-8 protein levels in macrophages. It also led to an increase in *IL-6* expression levels, above that induced by PMA³⁹. These results suggest a substantial, in vitro, pro-inflammatory role for F_{CBD} in macrophages. However, $F_{\text{CBD:std}}$ was less active in ILs induction, again demonstrating a notable difference between F_{CBD} and $F_{\text{CBD:std}}$, which may originate from the presence or absence, respectively, of terpenes.

To conclude, treatment with cannabis compounds CBD, CBG and THCV may have clinical value in reducing cytokine secretion in lung epithelial cells. However, treatment with F_{CBD} containing terpenes in addition to these phytocannabinoids substantially induced macrophage phagocytosis and increased their IL levels. Yet, to confirm more specifically the pro-inflammatory effect of F_{CBD} in macrophages it is necessary to perform the same experiments on primary alveolar macrophages (e.g., from mice). Nevertheless, these results suggest a pro-inflammatory role for cannabis extract that is higher than that of the phytocannabinoid standard mix. The latter maintained anti-inflammatory activity in the alveolar epithelial cells with relatively reduced pro-inflammatory activity in macrophages. Hence, the mix of phytocannabinoids shows superior activity versus the

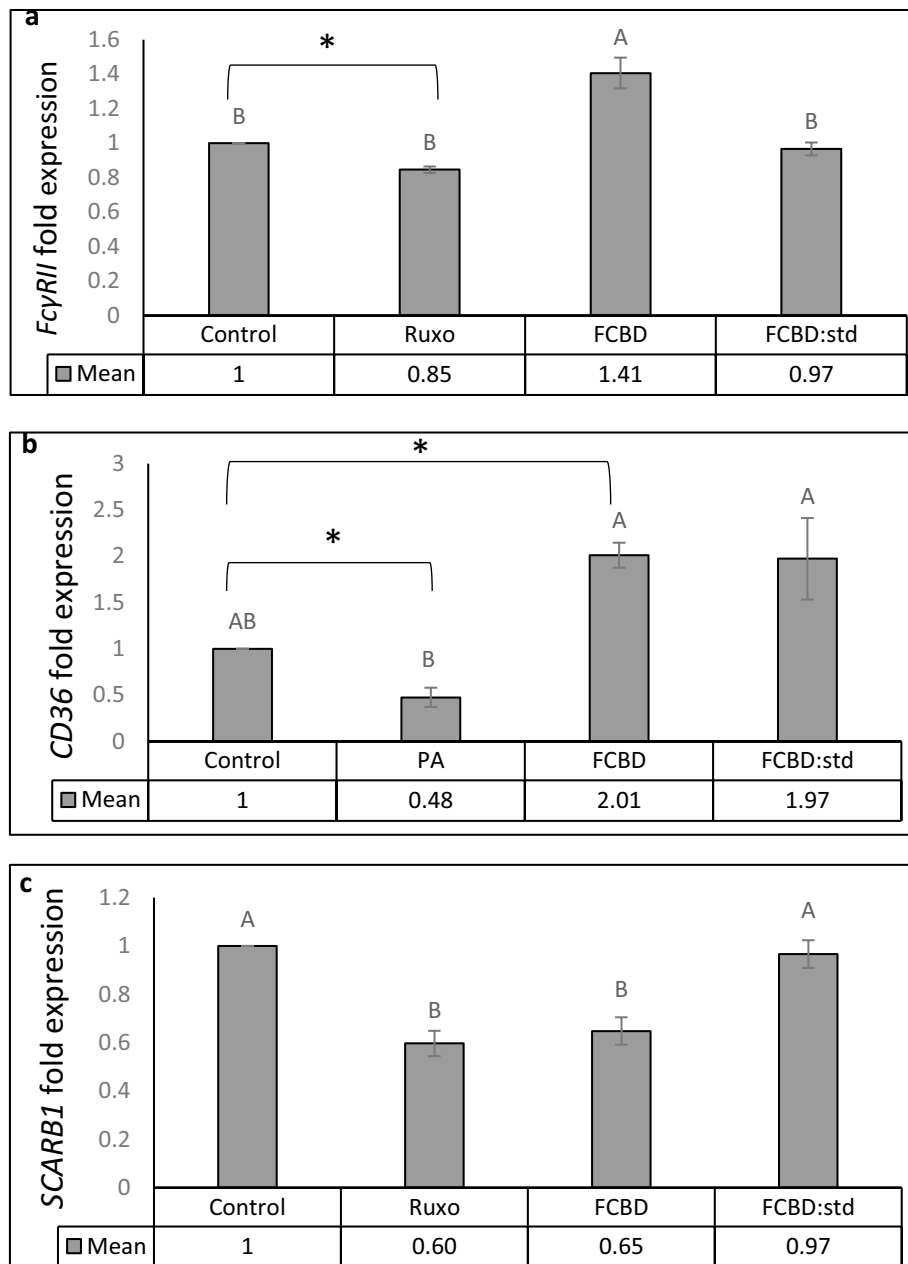


Figure 7. qPCR-based determination of the mRNA steady state level in the differentiated KG1 cell line. (a) *FcyRII*, (b) *CD36* or (c) *SCARB1* genes, after treatment with F_{CBD} (FCBD) at 7 $\mu\text{g}/\text{mL}$, $F_{CBD:std}$ (FCBD:std) at 7 $\mu\text{g}/\text{mL}$, ruxolitinib (Ruxo) at 100 $\mu\text{g}/\text{mL}$ or palmitic acid (PA) at 150 μM . In this experiment, controls (vehicle) for (a) and (c) were 0.7% v/v methanol + 2% v/v DMSO; for (b) 0.7% v/v methanol. Error bars indicate \pm sem ($n=3$). Bars labeled with different letters are significantly different from all combinations of pairs according to the Tukey–Kramer HSD test ($P \leq 0.05$). *Indicates significantly different mean from the control based on the Student T-test ($P \leq 0.05$).

cannabis-derived fraction. Although more studies are needed of cannabis treatment in COVID patients, there needs to be caution in proposing cannabis treatment for these patients, as is presently being suggested in the media. The increase of macrophage-secreted IL-6 and IL-8 levels by cannabis-based treatment may potentially lead to a worsening of the "cytokine storm" identified in severe COVID-19 patients. It should be stressed, in agreement with Pastor et al.⁴⁰, that for now, users and healthcare personnel should avoid the use of cannabis for COVID-19 prevention or treatment.

Treatment	FNP	ENP	ENPG
Control	100.0 ^b	100.0 ^a	100.0 ^a
F _{CBD}	147.8 ± 13.4 ^a	167.9 ± 11.2 ^a	132.9 ± 30.3 ^a
F _{CBD:std}	99.8 ± 0.8 ^b	125.3 ± 10.2 ^a	116.2 ± 3.1 ^a
CBD	118.85 ± 5.10 ^{ab}	121.3 ± 24.0 ^a	89.6 ± 3.9 ^a

Table 3. Percentage of macrophage cells out of the control with internalized FNP silica beads, presence of ENP and ENPG silica beads analyzed using imaging flow cytometry, following treatment with F_{CBD} at 7 µg/mL, F_{CBD:std} at 7 µg/mL, CBD at 4.35 µg/mL, or the control. Control (0.7% v/v methanol) treatment served as the solvent (vehicle) control. Fluorescein labeled silica particles (FNP: 50–100 nm, ENP: 30–70 nm, ENPG: 30–70 nm coated with IgG). At least 4000–6000 cells for each treatment were analyzed and the distribution of cell internalization scores were plotted using Amnis IDEAS software (n = 2). Means in the same column labelled with different letters are significantly different from all combinations of pairs according to the Tukey–Kramer HSD test (P ≤ 0.05).

Material and methods

Extract preparation. High CBD *Cannabis sativa* strain Arbel (IMC, Israel) inflorescence was extracted using ethanol as described previously⁴¹ and decarboxylated by heating the dried crude extract to 220 °C for 10 min. The dried decarboxylated extract was weighed, and then resuspended in absolute methanol (volume of solvent added according to the desired concentration) and filtered through a 0.45 µm syringe filter.

Extract fractionation. A flash chromatography apparatus equipped with a diode array detector was used to fractionize the decarboxylated crude extract. An Ecoflex C-18 80 g (Flash Pure, Buchi, C-18, 50 µm spherical, max. pressure 180 psi) column was used for separation, with methanol and water as the mobile phase, as suggested by the manufacturer.

Chemical analyses. HPLC and gas chromatograph with mass selective detector (GCMS 8860 and GC/MSD 5977B, Agilent) analysis was carried out as previously described⁴¹. Qualitative and quantitative analysis of the phytocannabinoids in fractions was done in comparison to the standard calibration curves obtained from dissolving standards in methanol at different concentrations from 0 to 25 µg/mL.

Standard/material preparation and use. The cannabinoid standards at a concentration of 1 mg/mL in methanol used in this study included cannabidiol (CBD, Restek catalog no. 34011) cannabigerol (CBG, Restek catalog no. 34091) and tetrahydrocannabivarin (THCV, Restek catalog no. 34100). Inverse agonists (IA) to cannabinoid receptors type 1 (CB1) and 2 (CB2) used were Abcam products: CB1 (AM251, ab120088), CB2 (SR144528, ab146185), as was the TRPA1 blocker (HC-030031, ab120554). All IAs, as well as the TRPV1 antagonist (Abcam ab141772) and TRPV2 antagonist (Tranilast 1098/10) were dissolved in dimethyl sulfoxide (DMSO) at a concentration of 10 mM. Phorbol 12-myristate 13-acetate (PMA) (P1585; Sigma Aldrich, USA) was dissolved in DMSO at the stock concentration of 5 µg/mL. Dexamethazone (D4902; Sigma Aldrich, USA) was dissolved in methanol at the stock concentration of 1000 µg/mL. Ruxolitinib JAKAVI was dissolved in DMSO at the concentration of 5000 µg/mL, confirmed with GCMS and HPLC and was used at a final concentration of 2% (v/v). TNFα (300-01A; PeproTech, Rocky Hill, NJ, USA) was dissolved in water at the stock concentration of 100 µg/mL. (3-Aminopropyl) triethoxysilane (APTES), N-(3-Dimethylaminopropyl)-N(3-ethylcarbodiimide hydrochloride (EDC), and 5(6)- Carboxyfluorescein, 2-(4-Morpholino) ethanesulfonic acid (MES) were purchased from Sigma-Aldrich (USA). Analytical grade methanol was used at final concentration of 10% (v/v) according to the indicated concentration of the treatment. The highest methanol concentration in each experiment was used for vehicle control. Ultra-pure deionized water (MS grade) was used as received without further purification. Palmitic acid (PA, Sigma Aldrich; P0500, USA) was dissolved in methanol at the stock concentration of 0.5 mol/L and used at 150 µM.

Cell cultures. The lung cancer cell line A549 (ATCC[®] CCL-185[™]) was cultured in DMEM (01-055-1A, Biological Industries, Israel) growth media supplemented with 10% FBS, 1% glutamic acid, 1% pen-strep and plasmocin. Macrophage cell line KG1 (ATCC[®] CCL-246[™]) was cultured in IMDM (01-058-1A; Biological Industries, Israel) containing 20% FBS and 1% pen-strep and plasmocin. 10 ng/mL PMA in IMDM media supplemented with 5% FBS, 1% pen-strep and plasmocin was used as stimulating environment for the differentiation of KG1 cells. Differentiated cells with typical morphology were attached to the plate surface within 1–2 days of initiation⁴².

Determination of IL levels and cell viability. IL-6 and IL-8 levels were determined as described previously⁴³ with the following modifications: A549 cells were plated at 5 × 10⁴ cells per well in DMEM complete media (400 µL) in 24-well cell culture plate. They were allowed to attach and grow at 37 °C in air and 5% CO₂ in a humidified incubator overnight with complete DMEM, and then the media was replaced with serum free DMEM. Cell excitation was performed with 300 ng/mL TNFα. Treatments were performed with cannabis crude extract, fraction or combination of compounds together with 100 µL serum free DMEM. IL-6 and IL-8

secretion levels were analyzed after 4 or 6 h of incubation for A549 or KG1 cell lines, respectively. Supernatant samples were collected and tested using IL-6 and IL-8 ELISA kits (DY206 and DY208 respectively, R&D Systems, Minneapolis, MN, USA). Dexamethasone was used as a positive control. For cell viability, an Alamar Blue (resazurin) assay was performed on each well as described previously⁴³. For dose response assays, data points were connected by non-linear regression lines of the sigmoidal dose–response relation. GraphPad Prism version 6.1 (<https://www.graphpad.com/scientific-software/prism/>, GraphPad Software Inc., San Diego, USA) was employed to produce dose–response curves and IC50 doses were calculated using nonlinear regression analysis.

Salinization of silicon dioxide surfaces with APTES. To prepare the silica dispersion, 1 g of silica was added to 40 mL of methanol and stirred. Then, APTES (0.0045 mol) was slowly added to the solution. The reaction was carried out at ambient temperature for 45 min. After silanization, 50–100 nm or 30–70 nm particles were collected by centrifugation (9000 rpm, 10 min) washed 4 times with water, and dried at 35 °C under vacuum for 3 h⁴⁴.

Labeling of amine functionalized silica nanoparticles with 5(6)-carboxyfluorescein and IgG. Stock solutions of 1 mg of EDC were prepared separately in 1 mL of 0.1 M MES (pH 4.5–5) buffer. 100 mg of the amine functionalized silica nanoparticles were added to 600 µL of the MES buffer followed by 200 µL of the EDC. The mixture was vortexed for 10 min. Then 100 µL 5(6)-Carboxyfluorescein (1 mg/mL) only (for 50–100 nm FNP or 30–70 nm ENP nanoparticles) or 100 µL 5(6)-Carboxyfluorescein (1 mg/mL) and IgG (10 mg/mL; for 30–70 nm ENPG nanoparticles) solutions were added. The final solution was then mixed by vortex for 3 h at ambient room temperature. Subsequently, the mixture was centrifuged and rinsed with MES buffer to remove excess reactants. EDC was used as a cross-linker to chemically attach the carboxyl group of the 5(6)-Carboxyfluorescein molecule and producing an amine-reactive O-acylisourea. For the fluorescent-IgG labelled silica nanoparticles this intermediate product reacted with the amino groups of the silica nanoparticles to yield an amide bond, releasing fluorescent-IgG labelled silica nanoparticles and urea as a by-product⁴⁵. The fluorescent labelled (FNP or ENP) or fluorescent-IgG labelled (ENPG) silica nanoparticles were then dispersed again in the MES buffer for further analysis.

Cellular staining and confocal microscopy. Differentiated macrophages from KG1 cells (10×10^4 cells/plate; plated on the bottom of a glass cell culture dish) were incubated in 500 µL of 5% FBS-IMDM media with FNP, ENP or ENPG (40 µg/mL) and incubated at 37 °C for 4 h for phagocytosis. Macrophages that underwent phagocytosis were fixed with 3.7% formaldehyde solution and permeabilized with 0.1% Triton X-100 at room temperature. Fixed cells were blocked in PBS containing 1% bovine serum albumin. Cells were incubated with EasyProbes™ ActinRed 555 Stain for actin and Hoechst for nuclear staining (AP-FP032, GC-C057 respectively; ABP Bioscience Rockville, MD, USA). Cell microscopy and image acquisition was carried out using a Leica SP8 laser scanning microscope (Leica, Wetzlar, Germany), equipped with a 405, 488 and 552 nm solid state lasers, HCX PL APO CS 10×/0.40 or HC PL APO CS 63×/1.2 water immersion objectives (Leica, Wetzlar, Germany) and Leica Application Suite X software (LASX, Leica, Wetzlar, Germany). Hoechst, 5(6)-Carboxyfluorescein and ActinRed 555 emission signals were detected with PMT and HyD (hybrid) detectors in ranges of 415–490 nm, 500–535 nm and 565–660 nm, respectively.

Quantitative real-time PCR. Quantitative real time PCR (qPCR) was carried out as described previously⁴¹. Briefly, cells were treated with cannabis compounds or methanol (0.7% v/v) as vehicle control for 4 or 6 h. Cells were then harvested and total RNA was extracted. RNA was reverse-transcribed, primers were designed and PCR was performed. The expression of each target gene was normalized to the expression of *Hypoxanthine Phosphoribosyltransferase 1 (HPRT1)* mRNA in the $2^{-\Delta\Delta Ct}$ and is presented as the ratio of the target gene to HPRT1 mRNA, expressed as $2^{-\Delta Ct}$, where Ct is the threshold cycle and $\Delta Ct = Ct_{\text{Target}} - Ct_{\text{HPRT1}}$. Experiments were repeated three times. The primers were:

ACE2 (Gene ID: 59,272) (forward) 5'-AAGCACTCACGATTGTTGGG-3' (reverse) 5'-CACCCCAACTATCTCTCGCT-3';
CCL2 (Gene ID: 6347) (forward) 5'-AAGGAGATCTGTGCTGACCC-3' (reverse) 5'-GCTGCAGATTCTTGGGTTGT-3';
IL-6 (Gene ID: 3569) (forward) 5'-GAACTCCTTCTCCACAAGCG-3' (reverse) 5'-GAAGAGGTGAGTGGCTGTCT-3';
CCL7 (Gene ID: 6354) (forward) 5'-CACCCCTCCAACATGAAAGCC-3' (reverse) 5'-GGTGGTCCTTCTGTAGCTCT-3';
IL-7 (Gene ID: 3574) (forward) 5'-CTGAAAGTACTGCTGGCG-3' (reverse) 5'-GAGTTGCCGAGTCTGTGTTG3';
FCyR2A (Gene ID: 2212) (forward) 5'-GCC AAT TCC ACT GAT CCT GT-3' (reverse) 5'-CCTGGGGTT CAGAGTCATGT-3';
SCARB1 (Gene ID: 949) (forward) 5'-CTG TGG GTG AGA TCA TGT GG-3' (reverse) 5'-GTT CCA CTT GTC CAC GAG GT-3';
CD36 (Gene ID: 948) (forward) 5'-AGA TGC AGC CTC ATT TCC AC-3' (reverse) 5'-TGG GTT TTC AAC TGG AGA GG-3';
IL-8 (Gene ID: 3576) (forward) 5'-CAG GAA TTG AAT GGG TTT GC-3' (reverse) 5'-AAA CCA AGG CAC AGT GGA AC-3'.

Imaging flow cytometry. Differentiated macrophages from KG1 cells (10×10^5 cells/plate; seeded on 6-well plate culture dish) were replaced with 2 mL of 5% FBS-IMDM media with FNP, ENP, or ENPG (40 $\mu\text{g}/\text{mL}$) and incubated at 37 °C for 4 h for phagocytosis. The cells were detached from the surface of the plate using a trypsin 0.25%:EDTA 0.05% solution (03-052-1A, Biological Industries, Israel) for 3 min, washed with DMEM complete media, centrifuged and transferred to 50 μL cold PBS kept on ice.

Cells were analyzed by multispectral imaging flow cytometry (ImageStream markII flow cytometer; Amnis Corp, part of EMD Millipore, Seattle, WA, USA). Fluorescence intensity of the Fluorescein labeled silica beads was measured in channel 2 of the cytometer (480 nm ex, 560 nm em). An 60 \times magnification with Olympus UplanFLN 60 \times dry objective 0.9NA was used for all samples. At least 4000 cells were collected for each sample and data were analyzed using a dedicated image analysis software (IDEAS 6.2; AmnisCorp). Cells were gated for single cells using the area and aspect ratio features, and for focused cells using the Gradient RMS feature. Cropped cells were further eliminated by plotting the cell area of the bright field image against the Centroid X feature (the number of pixels in the horizontal axis from the left corner of the image to the center of the cell mask). Cells were further gated for cells that were positive (for ENP, ENPG or FNP). Because of their larger size, only FNP beads could be further analyzed for bead internalization vs. those attached to the cell surface. This was done using the intensity feature (the sum of the background-subtracted pixel values within the masked area of the image) and max pixel (the largest value of the subtracted background pixel). FNP internalization was calculated by the internalization feature, i.e. the ratio of the intensity inside the cell to the intensity of the entire cell, mapped to a log scale. To define the internal mask for the cell, the object mask of the brightfield image was eroded by 8 pixels. Cells with an internalization score higher than 0.33 were gated as cells with internalized FNP.

Statistical analysis. Data were processed using the JMP statistical package (https://www.jmp.com/en_us/home.html, SAS Inc, NC, USA). Comparisons between two groups were made using the Student's T-Test. Comparisons between more than 2 groups were made with analysis of variance (ANOVA) followed by Tukey–Kramer's honest significant difference (HSD) test as post hoc. Values are shown as mean \pm standard error (sem). P values ≤ 0.05 were considered significant.

Data availability

The datasets generated during and/or analysed during the current study are available from the corresponding author on reasonable request.

Received: 8 October 2020; Accepted: 3 January 2021

Published online: 14 January 2021

References

1. Mehta, P. *et al.* COVID-19: Consider cytokine storm syndromes and immunosuppression. *Lancet* **395**, 1033 (2020).
2. Shi, Y. *et al.* COVID-19 infection: The perspectives on immune responses. *Cell Death Differ.* **27**, 1451–1454 (2020).
3. Ruscitti, P., Berardicurti, O., Iagnocco, A. & Giacomelli, R. Cytokine storm syndrome in severe COVID-19. *Autoimmun. Rev.* **19**, 102562 (2020).
4. Gao, Y. *et al.* Diagnostic utility of clinical laboratory data determinations for patients with the severe COVID-19. *J. Med. Virol.* **92**, 791–796 (2020).
5. Hanuš, L. O., Meyer, S. M., Muñoz, E., Tagliatalata-Scafati, O. & Appendino, G. Phytocannabinoids: A unified critical inventory. *Nat. Prod. Rep.* **33**, 1357–1392 (2016).
6. Berman, P. *et al.* A new ESI-LC/MS approach for comprehensive metabolic profiling of phytocannabinoids in Cannabis. *Sci. Rep.* **8**, 1–15 (2018).
7. Aizpurua-Olaizola, O. *et al.* Evolution of the cannabinoid and terpene content during the growth of *Cannabis sativa* plants from different chemotypes. *J. Nat. Prod.* **79**, 324–331 (2016).
8. Oláh, A., Szekanecz, Z. & Bíró, T. Targeting cannabinoid signaling in the immune system: “High”-ly exciting questions, possibilities, and challenges. *Front. Immunol.* **8**, 1487 (2017).
9. Gonçalves, E. D. & Dutra, R. C. Cannabinoid receptors as therapeutic targets for autoimmune diseases: Where do we stand?. *Drug Discov. Today* **24**, 1845–1853 (2019).
10. Romano, B. *et al.* Pure Δ^9 -tetrahydrocannabinol and a *Cannabis sativa* extract with high content in Δ^9 -tetrahydrocannabinol inhibit nitrite production in murine peritoneal macrophages. *Pharmacol. Res.* **113**, 199–208 (2016).
11. Friedman, M., Cepero, M. L., Klein, T. & Friedman, H. Suppressive effect of Δ^9 -tetrahydrocannabinol in vitro on phagocytosis by murine macrophages. *Proc. Soc. Exp. Biol. Med.* **182**, 225–228 (1986).
12. Lowin, T. *et al.* Cannabidiol (CBD): A killer for inflammatory rheumatoid arthritis synovial fibroblasts. *Cell Death Dis.* **11**, 1–11 (2020).
13. Byrareddy, S. N. & Mohan, M. SARS-CoV2 induced respiratory distress: Can Cannabinoids be added to anti-viral therapies to reduce lung inflammation?. *Brain Behav. Immun.* **87**, 120–121 (2020).
14. Ahmed, A. *et al.* Ruxolitinib in adult patients with secondary haemophagocytic lymphohistiocytosis: An open-label, single-centre, pilot trial. *Lancet Haematol.* **6**, e630–e637 (2019).
15. Hua, W. *et al.* CD36 mediated fatty acid-induced podocyte apoptosis via oxidative stress. *PLoS ONE* **10**, e0127507 (2015).
16. Gallily, R., Yekhtin, Z. & Hanuš, L. O. Overcoming the bell-shaped dose-response of cannabidiol by using cannabis extract enriched in cannabidiol. *Pharmacol. Pharm.* **6**, 75 (2015).
17. Laprairie, R., Bagher, A., Kelly, M. & Denovan-Wright, E. Cannabidiol is a negative allosteric modulator of the cannabinoid CB1 receptor. *Br. J. Pharmacol.* **172**, 4790–4805 (2015).
18. Mukhopadhyay, I. *et al.* Expression of functional TRPA1 receptor on human lung fibroblast and epithelial cells. *J. Recept. Signal Transduct. Res.* **31**, 350–358 (2011).
19. Müller, C., Morales, P. & Reggio, P. H. Cannabinoid ligands targeting TRP channels. *Front. Mol. Neurosci.* **11**, 487 (2019).
20. Li, M., Fan, X., Ji, L., Fan, Y. & Xu, L. Exacerbating effects of trimellitic anhydride in ovalbumin-induced asthmatic mice and the gene and protein expressions of TRPA1, TRPV1, TRPV2 in lung tissue. *Int. Immunopharmacol.* **69**, 159–168 (2019).
21. Merad, M. & Martin, J. C. Pathological inflammation in patients with COVID-19: A key role for monocytes and macrophages. *Nat. Rev. Immunol.* **20**, 355–362 (2020).

22. Remy, K. E. *et al.* Immunotherapies for COVID-19: Lessons learned from sepsis. *Lancet Respir. Med.* [https://doi.org/10.1016/S2213-2600\(20\)30217-4](https://doi.org/10.1016/S2213-2600(20)30217-4) (2020).
23. Levy, Y. *et al.* Enhanced T cell recovery in HIV-1-infected adults through IL-7 treatment. *J. Clin. Investig.* **119**, 997–1007 (2009).
24. Dalan, R. *et al.* The ACE-2 in COVID-19: Foe or friend?. *Horm. Metab. Res.* **52**, 257 (2020).
25. Li, F., Li, W., Farzan, M. & Harrison, S. C. Structure of SARS coronavirus spike receptor-binding domain complexed with receptor. *Science* **309**, 1864–1868 (2005).
26. Garvin, M. R. *et al.* A mechanistic model and therapeutic interventions for COVID-19 involving a RAS-mediated bradykinin storm. *elife* **9**, e59177 (2020).
27. Chen, J. *et al.* Individual variation of the SARS-CoV-2 receptor ACE2 gene expression and regulation. *Aging Cell* **19**, e13168 (2020).
28. Wang, C. *et al.* Alveolar macrophage dysfunction and cytokine storm in the pathogenesis of two severe COVID-19 patients. *EBioMedicine* **57**, 102833 (2020).
29. Yoshikawa, T., Hill, T., Peters, C. J. & Tseng, C.-T.K. Severe acute respiratory syndrome-Coronavirus (SARS-CoV)-induced lung epithelial cytokines exacerbate SARS pathogenesis by modulating intrinsic functions of monocyte-derived macrophages and dendritic cells. *J. Virol.* <https://doi.org/10.1128/JVI.01792-08> (2008).
30. Yasui, F. *et al.* Phagocytic cells contribute to the antibody-mediated elimination of pulmonary-infected SARS coronavirus. *Virology* **454**, 157–168 (2014).
31. Horsthemke, M. *et al.* Multiple roles of filopodial dynamics in particle capture and phagocytosis and phenotypes of Cdc42 and Myo10 deletion. *J. Biol. Chem.* **292**, 7258–7273 (2017).
32. Tsugita, M., Morimoto, N., Tashiro, M., Kinoshita, K. & Nakayama, M. SR-B1 is a silica receptor that mediates canonical inflammasome activation. *Cell Rep.* **18**, 1298–1311 (2017).
33. Greenberg, S. & Grinstein, S. Phagocytosis and innate immunity. *Curr. Opin. Immunol.* **14**, 136–145 (2002).
34. Wang, X., Lv, L., Chen, Y. & Chen, J. A CD36 synthetic peptide inhibits silica-induced lung fibrosis in the mice. *Toxicol. Ind. Health* **26**, 47–53 (2010).
35. He, W. *et al.* Alveolar macrophages are critical for broadly-reactive antibody-mediated protection against influenza A virus in mice. *Nat. Commun.* **8**, 1–14 (2017).
36. Huber, V. C., Lynch, J. M., Bucher, D. J., Le, J. & Metzger, D. W. Fc receptor-mediated phagocytosis makes a significant contribution to clearance of influenza virus infections. *J. Immunol.* **166**, 7381–7388 (2001).
37. Cooper, G. E. *et al.* Viral inhibition of bacterial phagocytosis by human macrophages: Redundant role of CD36. *PLoS ONE* **11**, e0163889 (2016).
38. Yip, M. S. *et al.* Antibody-dependent infection of human macrophages by severe acute respiratory syndrome coronavirus. *Virology* **11**, 1–11 (2014).
39. Navarro, S., Debili, N., Bernaudin, J., Vainchenker, W. & Doly, J. Regulation of the expression of IL-6 in human monocytes. *J. Immunol.* **142**, 4339–4345 (1989).
40. Pastor, F. P., Folgar, M. L., Carvalho, N., Carvalho, F. & Horcajadas, F. A. Therapeutic Cannabis and COVID-19: Between opportunism and infoxication. *Adicciones* **32**, 167–172 (2020).
41. Mazuz, M. *et al.* Synergistic cytotoxic activity of cannabinoids from cannabis sativa against cutaneous T-cell lymphoma (CTCL) in-vitro and ex-vivo. *Oncotarget* **11**, 1141 (2020).
42. Starr, T., Bauler, T. J., Malik-Kale, P. & Steele-Mortimer, O. The phorbol 12-myristate-13-acetate differentiation protocol is critical to the interaction of THP-1 macrophages with *Salmonella typhimurium*. *PLoS ONE* **13**, e0193601 (2018).
43. Nallathambi, R. *et al.* Anti-inflammatory activity in colon models is derived from δ 9-tetrahydrocannabinolic acid that interacts with additional compounds in cannabis extracts. *Cannabis Cannabinoid Res.* **2**, 167–182 (2017).
44. Yaakov, N. *et al.* Single cell encapsulation via pickering emulsion for biopesticide applications. *ACS Omega* **3**, 14294–14301 (2018).
45. Mani, K. A., Yaakov, N., Itzhaik Alkotzer, Y., Zelikman, E. & Mechrez, G. A robust fabrication method for amphiphilic Janus particles via immobilization on polycarbonate microspheres. *Polymers* **10**, 900 (2018).

Acknowledgements

We thank Zach Dunseth for English editing, Hillary Voet for statistical consultation and Dean Yoselewitz and Hadar Peeri for assistance in conducting the experiment.

Author contributions

S.M.A., A.C.V. and S.N. conducted experiments, N.S. designed experiments and analyzed the results, D.N. performed chemical analysis, E.B. performed microscopy examination, I.S. performed ImageStream analysis, K.A.M. conducted particle formation and labeling, G.M. managed particle formation and labeling and was involved with project conception, H.K. conceived the project, supervised the experiments and analysis, and wrote the manuscript. All authors read and approved the final draft of the manuscript.

Competing interests

The authors declare no competing interests.

Additional information

Supplementary Information The online version contains supplementary material available at <https://doi.org/10.1038/s41598-021-81049-2>.

Correspondence and requests for materials should be addressed to H.K.

Reprints and permissions information is available at www.nature.com/reprints.

Publisher's note Springer Nature remains neutral with regard to jurisdictional claims in published maps and institutional affiliations.



Open Access This article is licensed under a Creative Commons Attribution 4.0 International License, which permits use, sharing, adaptation, distribution and reproduction in any medium or format, as long as you give appropriate credit to the original author(s) and the source, provide a link to the Creative Commons licence, and indicate if changes were made. The images or other third party material in this article are included in the article's Creative Commons licence, unless indicated otherwise in a credit line to the material. If material is not included in the article's Creative Commons licence and your intended use is not permitted by statutory regulation or exceeds the permitted use, you will need to obtain permission directly from the copyright holder. To view a copy of this licence, visit <http://creativecommons.org/licenses/by/4.0/>.

© The Author(s) 2021